THE ASTROPHYSICAL JOURNAL, 883:61 (7pp), 2019 September 20

© 2019. The American Astronomical Society. All rights reserved.

https://doi.org/10.3847/1538-4357/ab3a37

NICER Observes a Secondary Peak in the Decay of a Thermonuclear Burst from 4U 1608–52

Gaurava K. Jaisawal[1], Jérôme Chenevez[1], Peter Bult[2], Jean J. M. in't Zand[3], Duncan K. Galloway[4,5],
Tod E. Strohmayer[6], Tolga Güver[7,8], Phillip Adkins[9], Diego Altamirano[10], Zaven Arzoumanian[2], Deepto Chakrabarty[11],
Jonathan Coopersmith[12], Keith C. Gendreau[2], Sebastien Guillot[13,14], Laurens Keek[15], Renee M. Ludlam[16], and
Christian Malacaria[17,18,19]

[1] National Space Institute, Technical University of Denmark, Elektrovej 327-328, DK-2800 Lyngby, Denmark; gaurava@space.dtu.dk
[2] Astrophysics Science Division, NASA's Goddard Space Flight Center, Greenbelt, MD 20771, USA
[3] SRON Netherlands Institute for Space Research, Sorbonnelaan 2, 3584 CA Utrecht, The Netherlands
[4] School of Physics & Astronomy, Monash University, Clayton VIC 3800, Australia
[5] Monash Centre for Astrophysics, Monash University, Clayton VIC 3168, Australia
[6] Astrophysics Science Division and Joint Space-Science Institute, NASA's Goddard Space Flight Center, Greenbelt, MD 20771, USA
[7] Department of Astronomy and Space Sciences, Science Faculty, Istanbul University, Beyazıt, 34119 Istanbul, Turkey
[8] Istanbul University Observatory Research and Application Center, Beyazıt, 34119 Istanbul, Turkey
[9] Safety Division, NASA's Goddard Space Flight Center, Greenbelt, MD 20771, USA
[10] Physics & Astronomy, University of Southampton, Southampton, Hampshire SO17 1BJ, UK
[11] MIT Kavli Institute for Astrophysics and Space Research, Massachusetts Institute of Technology, Cambridge, MA 02139, USA
[12] KBRwyle and Quality & Reliability Division, NASA's Goddard Space Flight Center, Greenbelt, MD 20771, USA
[13] CNRS, IRAP, 9 avenue du Colonel Roche, BP 44346, F-31028 Toulouse Cedex 4, France
[14] Université de Toulouse, CNES, UPS-OMP, F-31028 Toulouse, France
[15] Department of Astronomy, University of Maryland, College Park, MD 20742, USA
[16] Department of Astronomy, University of Michigan, 1085 South University Ave, Ann Arbor, MI 48109-1107, USA
[17] NASA Marshall Space Flight Center, NSSTC, 320 Sparkman Drive, Huntsville, AL 35805, USA
[18] Universities Space Research Association, NSSTC, 320 Sparkman Drive, Huntsville, AL 35805, USA
Received 2019 January 20; revised 2019 August 5; accepted 2019 August 8; published 2019 September 20

Abstract

We report for the first time below 1.5 keV, the detection of a secondary peak in an Eddington-limited thermonuclear X-ray burst observed by the *Neutron Star Interior Composition Explorer* (*NICER*) from the low-mass X-ray binary 4U 1608–52. Our time-resolved spectroscopy of the burst is consistent with a model consisting of a varying-temperature blackbody, and an evolving persistent flux contribution, likely attributed to the accretion process. The dip in the burst intensity before the secondary peak is also visible in the bolometric flux. Prior to the dip, the blackbody temperature reached a maximum of $\approx$3 keV. Our analysis suggests that the dip and secondary peak are not related to photospheric expansion, varying circumstellar absorption, or scattering. Instead, we discuss the observation in the context of hydrodynamical instabilities, thermonuclear flame spreading models, and reburning in the cooling tail of the burst.

Key words: accretion, accretion disks – stars: individual (4U 1608-52) – stars: neutron – X-rays: binaries – X-rays: bursts

1. Introduction

Thermonuclear (type I) X-ray bursts originate in the unstable burning of hydrogen- or helium-rich material on the surface of a neutron star (for reviews, see Lewin et al. 1993; Strohmayer & Bildsten 2003; Galloway & Keek 2017). This material is typically accreted from a (sub)solar mass companion through Roche-lobe overflow in low-mass X-ray binaries (LMXBs). Type-I X-ray bursts (simply bursts hereafter) are characterized by a few-second rise in X-ray luminosity by at least an order of magnitude and lasting tens to hundreds of seconds. Their X-ray emission during the decaying part of the burst is consistent with a cooling blackbody with a 2–3 keV peak temperature. It is commonly assumed that the "persistent" emission from the accretion process remains constant during the burst. However, recent studies suggest that the irradiation from bursts can modify the persistent continuum (Chen et al. 2012; in't Zand et al. 2013; Worpel et al. 2013, 2015; Degenaar et al. 2018; Keek et al. 2018a). These effects can be interpreted as reprocessing/reflection from the disk (Ballantyne 2004),

changes in the accretion flow rate through Poynting–Robertson drag (Walker 1992), or cooling of the corona (Ji et al. 2014b).

The most luminous bursts reach the Eddington limit: the outward radiation pressure overcomes the gravitational binding energy, leading to photospheric radius expansion (PRE; Ebisuzaki et al. 1983; Lewin et al. 1984). PRE bursts show a sudden drop in temperature and an increase in the photospheric radius by tens of kilometers above the surface (Kuulkers et al. 2003; Keek et al. 2018b). As it expands, the photosphere cools causing its thermal spectrum to shift to lower energies, and possibly out of the passband of hard X-ray instruments such as those flown on the *Rossi X-ray Timing Explorer* (*RXTE*) and *INTEGRAL*. This spectral shift causes a drop in the measured intensity for these instruments. Following its expansion phase, the photosphere falls back onto or close to the neutron star surface, heats up, and its thermal spectrum therefore reenters the hard X-ray band, causing a secondary increase of the measured intensity. This passband limitation of hard X-ray instruments is usually responsible for the double-peaked structure observed, while the bolometric flux is single-peaked (Fujimoto & Gottwald 1989; Galloway et al. 2008).

---

[19] NASA Postdoctoral Fellow.

Some sources such as 4U 1636–536 (Bhattacharyya & Strohmayer 2006) and GX 17+2 (Kuulkers et al. 2002) are known to show intrinsically double-peaked bursts. Despite the fact that these events were non-PRE bursts, their bolometric flux contained a dip-like structure. The Rapid Burster is another example where six double-peaked type-I (non-PRE) bursts have been detected during the soft to hard state transition (Bagnoli et al. 2014). A very rare triple-peaked burst is also known from 4U 1636–536 (Zhang et al. 2009).

In this paper, we study the flux and spectral evolution of a burst that included a second peak during its cooling tail, as observed from the atoll source 4U 1608–52 using the *Neutron Star Interior Composition Explorer* (*NICER;* Gendreau et al. 2016; Gendreau & Arzoumanian 2017).

The X-ray burster 4U 1608–52 is a well-known transient LMXB that was discovered in 1971 with two *Vela-5* satellites (Belian et al. 1976; Grindlay & Gursky 1976; Tananbaum et al. 1976). The neutron star in the system accretes from the late F- or early G-type star QX Nor—a source rich in hydrogen and helium—in an orbit of period 0.537 days (Grindlay & Liller 1978; Wachter et al. 2002).

4U 1608–52 moves through different accretion states during an outburst. At low luminosities, the source is in the so-called hard spectral state, where its spectrum is dominated by a hard power-law component. At higher luminosities, the accretion-disk transitions to the soft state and exhibits a spectrum dominated by soft thermal photons (see, e.g., Done et al. 2007 for spectral state classification). 4U 1608–52 usually shows bursts in both the soft (banana branch) and hard (island) states. Ji et al. (2014a) showed that the bursts affect the persistent emission differently based on the spectral state. The persistent flux observed in the soft state increases across the burst, while this behavior holds in the hard state only when the burst is non-PRE. A decreasing persistent flux is observed for brighter events in the hard state (Ji et al. 2014a).

Thanks to observations of PRE bursts, the source distance is known to lie within the range 2.9–4.5 kpc (Galloway et al. 2008; Güver et al. 2010). The spin period is constrained to ≈620 Hz based on the detection of burst oscillations (Muno et al. 2001; Galloway et al. 2008). Other physical parameters of the neutron star determined from burst time-resolved spectroscopy are a mass $M = 1.2$–$1.6\ M_\odot$ and a radius of 13–16 km (Poutanen et al. 2014; see also Özel et al. 2016). In addition to regular bursts, one superburst, likely due to the deep burning of a thick carbon layer, was observed in 2005 (Keek et al. 2008).

Using high timing and spectral capabilities of *NICER* in soft X-rays, we study a double-peaked burst from 4U 1608–52 for the first time below 1.5 keV. The present paper focuses on the nature of this event and also examines the effect of the burst emission on the accretion environment using a variable persistent flux method. We describe the observations and our analysis methods in Section 2, and present our results and discussion in Sections 3 and 4, respectively.

2. Observations and Analysis

Launched in 2017 June, the *NICER* X-ray Timing Instrument (XTI; Gendreau et al. 2016) is a nonimaging soft X-ray telescope attached to the International Space Station. It consists of 56 coaligned concentrator optics, each paired with a silicon-drift detector (Prigozhin et al. 2012). This instrument records photons between 0.3 and 12 keV at an unprecedented time resolution of ≈100 ns and spectral resolution of ≈100 eV (full
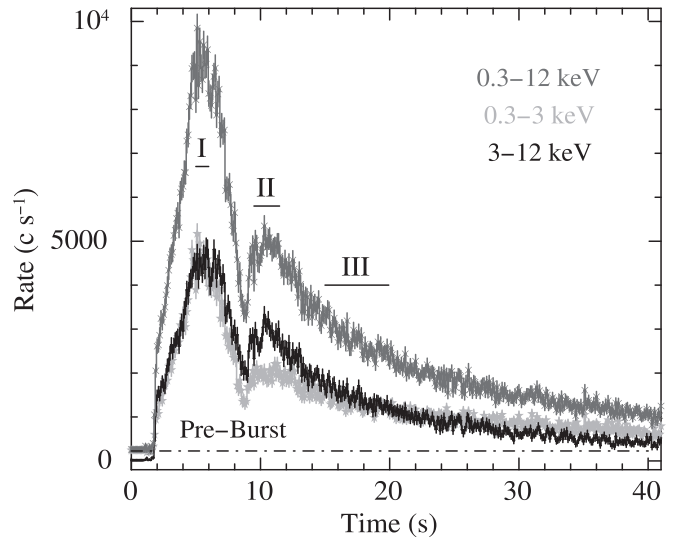

Figure 1. Burst light curve observed with *NICER* at 0.1 s resolution. A rebrightening is detected at all energies ≃5 s after the primary peak. The preburst count rate (horizontal line) is ∼226 c s⁻¹ in the 0.3–12 keV band. The segments I, II, and III represent broad time spans used for time-resolved spectroscopy at the first peak, second peak, and in the decay part of the burst, respectively.

width at half maximum). The peak effective area of the 52 currently active detectors is ≈1900 cm² at 1.5 keV.

NICER monitored the transient source 4U 1608–52 actively as part of the mission's baseline science program. Only two type-I bursts have been observed (in publicly available data sets ObsID 0050070101–0050070110, 1050070101–1050070174, and 2050070101–2050070111) over a net exposure of 180.3 ks in between 2017 June and 2019 April. The first burst was observed on 2017 June 25 (MJD 57929.5002, ObsID: 0050070102), reaching a peak intensity of 6230 ± 250 c s⁻¹ in the 0.3–12 keV band, whereas the second was detected on 2017 September 28 (MJD 58024.2294, ObsID: 1050070103), peaking at 9840 ± 306 c s⁻¹. The latter event is the focus of the present study.

We processed the data using HEASOFT version 6.24, NICERDAS version 2018-04-24_V004, and the calibration database version 20180711. Good time intervals (GTIs) were created via NIMAKETIME using the standard filtering criteria. We applied these GTIs on processed XTI data to produce the spectra and light curves. For the spectral study, we used XSPEC version 12.10.0 (Arnaud 1996) along with *NICER* response and effective area files version 1.02. The background contribution to our observations is determined from *NICER* observations of an *RXTE* blank-sky region (∼1–2 c s⁻¹ from *RXTE*-6; Jahoda et al. 2006).

3. Results

3.1. Burst Light Curve

Figure 1 shows 0.1 s binned light curves of the burst detected by *NICER* on 2017 September 28 (MJD 58024.2294), in the 0.3–12 keV, 0.3–3 keV, and 3–12 keV bands. The intensity remained above 20% of the peak count rate for ≃20 s. The burst reached a maximum count rate of 9840 c s⁻¹ (0.3–12 keV) 3.5 s after onset. About 5 s later, after a dip, a second peak at 5200 c s⁻¹ occurred in the burst tail (Figure 1). The observed count rate of the first peak was nearly the same in the 0.3–3 and 3–12 keV energy bands, while the second peak was
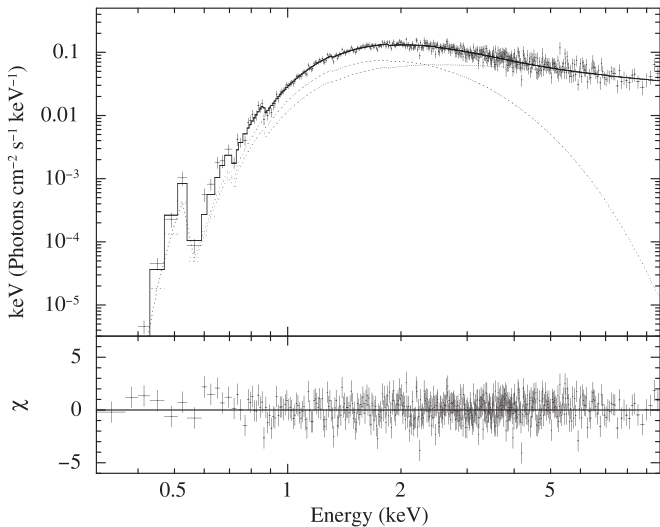
Figure 2. *NICER* spectrum from the persistent emission prior to the burst. In the top panel the 0.3–10 keV energy spectrum is well described by an absorbed disk-blackbody plus a power-law model. Spectral residuals corresponding to the best-fitting model are shown in the bottom panel.
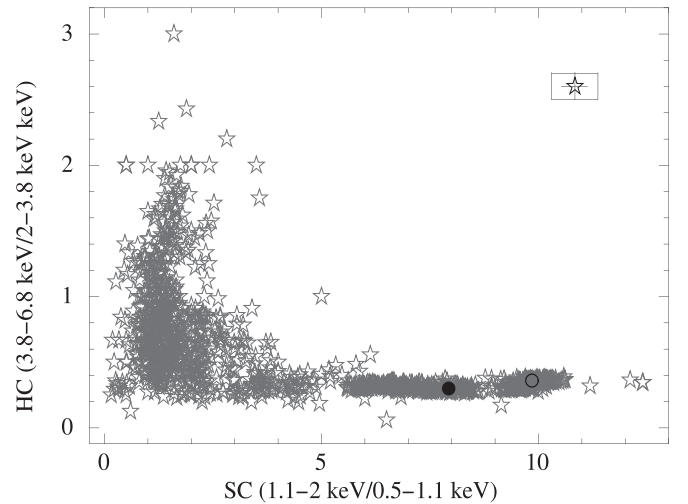

Figure 3. *NICER* color–color diagram of 4U 1608–52 observed between 2017 June and 2019 April. The soft color (SC) is defined as the ratio of count rates in the (1.1–2.0)/(0.5–1.1) keV energy bands, whereas the hard color (HC) is from the ratio of count rates in the (3.8–6.8)/(2.0–3.8) keV energy bands. Each point indicates a binning time of 128 s with typical error bars as shown in the right corner of the figure. The position of the two bursts observed by *NICER* are indicated by circles in the banana branch. Thus the source spectral state was soft during the present double-peaked burst (solid circle).

comparatively fainter in the soft ($\leqslant$3 keV) X-rays. The dip observed between the two peaks reached a minimum count rate of $\approx$3330 count s^{-1} in the full *NICER* band.

We searched for burst oscillations between 612 and 626 Hz with a resolution of $1/8192$ s in the 0.5–8.5 keV data starting from 20 s prior to burst onset, in sliding windows of $T = 2, 4$ and 8 s striding at a pace of $T/2$. No burst oscillations were observed near either peak of the X-ray burst to an upper limit of 8% fractional amplitude.

3.2. Persistent Emission

The burst considered in this paper occurred 210 s into the third GTI of ObsID 1050070103. We accumulated the first 165 s of good data prior to the onset of the burst for the preburst emission. The energy spectrum extracted from this interval was fitted with a disk-blackbody (`diskbb`) model (Mitsuda et al. 1984) along with a power-law component. The full model `TBabs × (diskbb + power-law)` is able to describe the 0.3–10 keV persistent spectrum reasonably well (Figure 2). The goodness of fit per degree of freedom is found to be $\chi^2/\nu = \chi^2_\nu = 1.05$ for $\nu = 468$ degrees of freedom. The interstellar medium absorption $N_{\rm H}$ is described by `TBabs` (Wilms et al. 2000). We found a column density of $(0.98 \pm 0.03) \times 10^{22}$ cm^{-2} with *NICER*, which is well within the 1σ uncertainty reported by Keek et al. (2008) and Özel et al. (2016). We do not detect any Fe line feature in the preburst continuum.

The spectral parameters of our best-fit model and their 1σ errors are an inner disk temperature $T_{\rm in}$ of the disk blackbody of $kT_{\rm in} = 0.65 \pm 0.03$ keV, an inner disk radius $R_{\rm in}$ of the disk blackbody given by $(R_{\rm in}/D_{\rm 10\,kpc})^2 \cos\theta = 193 \pm 25$ km^2, where $D_{\rm 10\,kpc}$ is the distance to the source in units of 10 kpc, a photon index of the power law of $\Gamma = 1.6 \pm 0.2$ and a normalization of the power law at 1 keV of 0.14 ± 0.04 phot s^{-1} keV^{-1} cm^{-2}. We used the `cflux` model to compute the unabsorbed flux in the 0.3–10 keV band, which was found to be $(1.75 \pm 0.02) \times 10^{-9}$ erg s^{-1} cm^{-2}. By extrapolating beyond the *NICER* energy range, the unabsorbed 0.1–100 keV band bolometric flux was estimated to be $(2.4 \pm 0.1) \times 10^{-9}$ erg s^{-1} cm^{-2}. We quote only unabsorbed fluxes in

this paper. At this flux, 4U 1608–52 was accreting at a persistent level of $\approx$1.6% of Eddington luminosity. This is calculated with respect to the maximum flux $(1.5 \times 10^{-7}$ erg s^{-1} cm^{-2}; Galloway et al. 2008) observed by *RXTE* as the Eddington limit.

We attempted to determine the spectral state before the burst using different methods as follows. First, a timing approach was adopted on the *NICER* data (van Straaten et al. 2003). This was done by comparing the source power spectrum, energy spectrum, and bolometric luminosity of the persistent emission with archival *RXTE* observations of 4U 1608–52 (van Straaten et al. 2003). The analysis suggested that the source was possibly in the intermediate lower-left banana branch at the time of the burst. We also quantified the spectral state of the burst in the color–color diagram as shown in Figure 3. This diagram is obtained by using the available *NICER* observations between 2017 June and 2019 April at various accretion states. In our analysis, the soft color (SC) is defined as the ratio of count rates in the (1.1–2.0)/(0.5–1.1) keV energy bands, while the hard color (HC) is obtained by the ratio of count rates in the (3.8–6.8)/(2.0–3.8) keV energy bands (see, e.g., Bult et al. 2018). Based on the colors prior to the burst (solid circle in Figure 3), the double-peaked event seems to have occurred in the lower banana branch of this atoll source.

3.3. Time-resolved Spectroscopy of the Burst

To investigate the temporal evolution of the burst spectrum, we first divide the burst light curve into three broad time segments: we use a 1 s bin on the first peak; a 2 s bin on the second peak; and a 5 s bin in the tail of the X-ray burst (Figure 1). The 0.3–10 keV spectra from these three segments were modeled with a blackbody (`bbodyrad` in *XSPEC*) component after subtracting the preburst emission as a background component. The column density for interstellar absorption was kept fixed at the value obtained for the persistent emission (Section 3.2). We noticed that this model is not sufficient to adequately describe the continuum, especially for the burst peak where strong excesses are seen at both ends
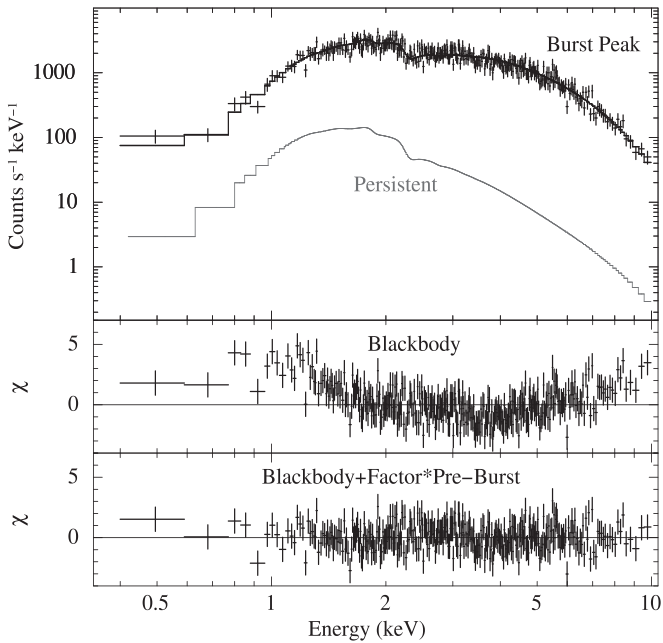
Figure 4. The 0.3–10 keV *NICER* spectrum obtained from a 1 s time interval at the burst peak. The best-fitting model, shown in the top panel, comprises an absorbed blackbody along with scaled preburst (persistent) emission. The middle panel shows the residuals corresponding to a simple blackbody model after subtracting the preburst emission, while the bottom panel shows the residuals for the best-fitting f_a model. See Section 3.3 for details.

Figure 5. Evolution of spectral parameters obtained from burst time-resolved spectroscopy. The top panel shows the burst light curve at 0.05 s time resolution. The vertical dotted line marks the minimum of the dip feature. The second, third, fourth, and fifth panels show the temperature, blackbody radius for a distance of 4 kpc, scale factor f_a and reduced-χ^2, respectively. The horizontal dotted line in the fourth panel is marked at the unity.

of the bandpass (second panel of Figure 4). The corresponding goodness of fit $\chi^2(\nu)$ was found to be 830(506), 633(552), and 622(577) for the first, second, and third time segments, respectively.

A better description of the burst emission was obtained by using the variable persistent flux method (Worpel et al. 2013). For this method, we used a blackbody component in addition to the fixed preburst spectral model obtained from the analysis of the persistent emission (Section 3.2), together with a free multiplicative factor f_a in the following way: `TBabs ×` `(bbodyrad+`f_a`× (diskbb + power-law))`. The scale factor f_a accounts for variation in the persistent continuum level with respect to the preburst value. However, we note that the burst emission, in general, can deviate from pure blackbody radiation due to the effect of the neutron star's atmosphere and its fast rotation (see, e.g., Suleimanov et al. 2012). Thus, the variation in f_a likely represents a net outcome from the atmosphere as well as a possible contribution from the varying accretion flow during the burst. Our current understanding hardly allows us to segregate these effects from the spectrum due to degeneracy in theoretical modeling (Worpel et al. 2015; Degenaar et al. 2018). Using the above method, we obtain an improved fit with $\chi^2(\nu) = 577(505)$, 624(551), and 616(576) for the first, second, and third time segments, respectively. The residuals corresponding to the burst peak interval are shown in the third panel of Figure 4. From this preliminary analysis, we find variation in the blackbody temperature, normalization, and f_a across the burst, motivating a more detailed analysis.

In addition to the above spectral modeling, various absorption components such as partial covering (`pcfabs`), absorption through warm (`wndabs`), neutral, and partially ionized materials (`zxipcf`) were also applied in the variable persistent flux, especially on a spectrum extracted from a 0.7 s interval at the dip phase, in order to constrain possible origins
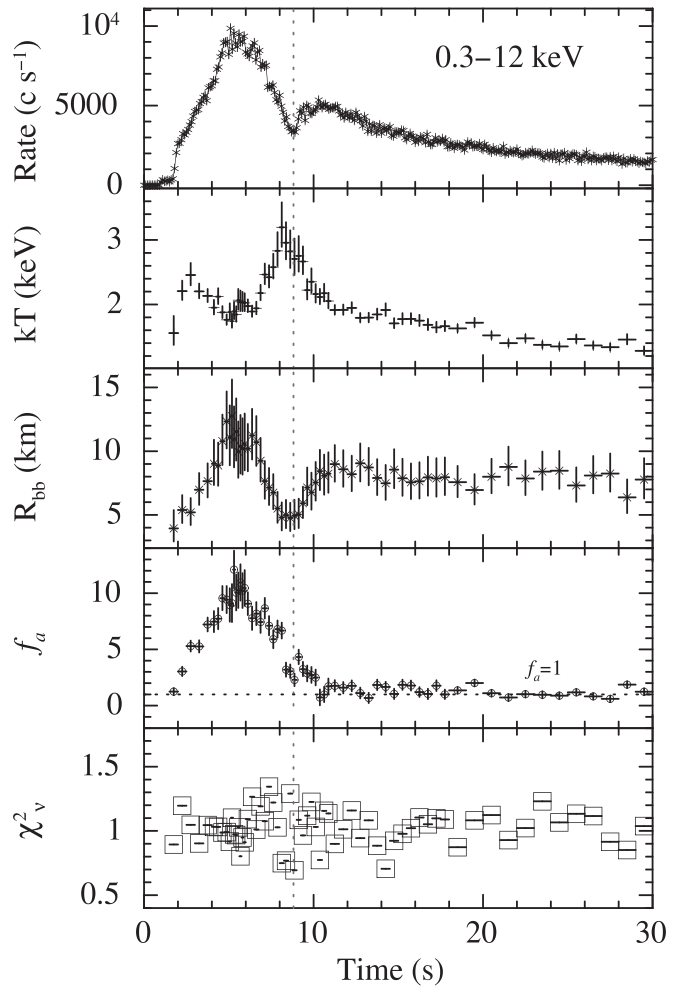
of the dip in an obscuring medium present close to the neutron star surface. None of these models fitted significantly better than the f_a model with interstellar absorption with N_H fixed to 0.98×10^{22} cm^{-2} as found from the persistent spectrum, nor do these models provide evidence for increased absorption due to (partially ionized) gas.

Next, we explored time-resolved spectroscopy on a finer timescale in order to more fully probe the burst evolution and understand the origin of the two peaks (or the one dip) in the profile. For this, we extracted a total of 63 spectra with a duration of at least 0.125 s allowing >1000 counts per spectrum. We fitted all the spectra with the variable persistent flux model as described above. The results show that the blackbody radius expands during the peak of the burst (Figure 5). Considering a distance of 4 kpc (Güver et al. 2010), the maximum expansion radius R_{bb} is estimated to be 12 ± 2 km (mean-weighted value from six points on the peak) using the blackbody normalization (third panel of Figure 5). In contrast to the expansion, the blackbody temperature drops to a value of 1.83 ± 0.07 keV after the burst onset (second panel of Figure 5). At the same time, the bolometric flux reaches, during one second, a plateau consistent with the Eddington flux, at
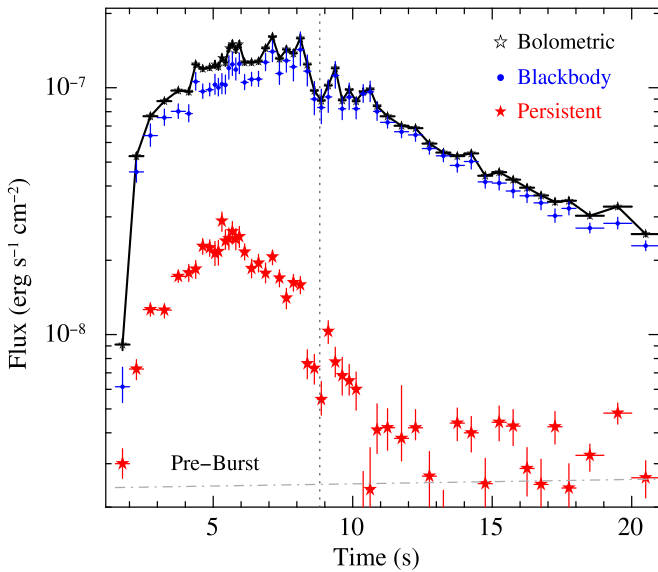
Figure 6. Evolution of the 0.1–100 keV bolometric, blackbody, and persistent fluxes during the burst. The vertical line shows the time when the dip occurs in the light curve, while the horizontal line marks the preburst flux level.

$(1.4 \pm 0.2) \times 10^{-7}$ erg s^{-1} cm^{-2} for the peak (Figure 6). The measured flux is in the same range as the brightest PRE events seen from 4U 1608–52 with *RXTE* (Galloway et al. 2008).

A gradual increase in blackbody temperature was noticed after the photospheric expansion (second panel of Figure 5). The temperature reaches $\approx 3.2 \pm 0.4$ keV during this phase. We found that the dip observed in the light curve does not coincide with the maximum temperature, but appears late by about 0.75 s. Given this time shift, we suggest that the observed dip is unlikely to be related to PRE or any limitation of the instrument passband. A final cooling trend is observed ≈ 8 s after the burst onset.

An unusual drop in bolometric flux is detected at the dip with a significance level of $\approx 3.5\sigma$ (Figure 6). This dip reaches a flux value of $(8.8 \pm 0.3) \times 10^{-8}$ erg s^{-1} cm^{-2}. Such a drop can also be seen in the evolving persistent level. It is interesting to point out that the bolometric flux rebrightens ~ 1 s earlier than the second intensity peak in the light curve. The scaling factor f_a shows a noticeable variation, reaching up to a value of 13 during the first peak, and returning to unity within nine seconds after onset as shown in Figure 5.

4. Discussion and Conclusions

In this paper, we discuss the results of a strong, double-peaked burst observed from 4U 1608–52 using *NICER*. Secondary peaks in the burst decay were detected in the soft X-ray light curves, as well as in the bolometric flux. Correspondingly, a dip between the first and second peaks is also visible in our study. It is worth noting that this dip shows a clear offset with the highest blackbody temperature in the burst tail, excluding the possibility of the feature being of instrumental origin, as discussed in Section 1. To date, a number of strong PRE bursts have been recorded by *NICER* in sources like, e.g., 4U 1820–30. In these cases the 0.3–12 keV burst profile is singly peaked despite a maximum color temperature of ≈ 4 keV appearing in the cooling tail (e.g., Keek et al. 2018b). Based on the above analogy, we

argue that the present double-peaked burst from 4U 1608–52 is of astrophysical origin.

A similar double-peaked burst from 4U 1608–52 in the low state was seen by *EXOSAT* in the 1.4–20 keV band (Figure 1 of Penninx et al. 1989). It was a 30 s long event with a peak intensity 1.35×10^{-7} erg s^{-1} cm^{-2}, similar to the present burst. The second peak of the *EXOSAT* burst was detected $\simeq 3$ s after the first peak, while with the *NICER* burst the rebrightening occurred about 5 s after the first peak. Moreover, a bolometric flux dip was also clearly found in the *EXOSAT* burst. Penninx et al. (1989) explained the double-peaked burst by considering multiple generations or release of thermonuclear energy. They also considered the possibility of absorption and scattering from an accretion-disk corona that could have produced a dip in the burst profile. Similar bursts with a flux drop have also been observed with *RXTE* (e.g., burst number 12 and 17 in Figure 1 of Poutanen et al. 2014), establishing the fact that double-peaked bursts are occasionally seen in 4U 1608–52 irrespective of instrumentation.

Given the similarity, we have examined the relevant hypotheses above as potential explanations for the double-peaked burst observed with *NICER*. The effects of transient absorption through a disk corona, hot medium, or a variable spreading layer (Penninx et al. 1989; Kajava et al. 2017) were explored with detailed spectral analysis. We did not find any evidence of additional absorbers at the dip intervals. Thus, absorption/scattering of X-ray photons is not a satisfying solution for the observed dip. We suggest instead that the peak following the dip in flux is due to enhanced emission in the cooling tail.

The thermonuclear flame spreading model of non-PRE bursts can explain the origin of a double-peaked burst (Bhattacharyya & Strohmayer 2006). According to this model, the burning starts at high latitude on the stellar surface and propagates toward the equator. When the flame reaches the equator, it stalls for a few seconds before spreading into the other hemisphere. The stall allows the stellar surface to cool down, causing the observed burst flux to temporarily decrease. After a few seconds, the flame continues to spread over the remaining surface, producing a secondary rise in flux. While this model describes the phenomenological shape of the burst light curve, it is unclear what physical mechanism would cause the burning front to stall. A potential explanation may be related to the interaction between the burning front and the spreading flow of accreted matter (Inogamov & Sunyaev 1999; Bhattacharyya & Strohmayer 2006).

Alternatively, reburning of fresh or leftover material (see, e.g., Keek & Heger 2017 and references therein) may produce the second peak in the cooling tail of a burst. It is not clear how the fresh material can be kept aside without mixing with burnt fuel (Spitkovsky et al. 2002); however, it has been suggested that a hydrodynamical shear instability induced by convection during the thermonuclear explosion could lead to accumulation of fresh fuel above the burnt material (Fujimoto et al. 1988). A model based on nuclear waiting points in the rp-process can also explain the double-peaked structure, for accretion rates of a few percent of $\dot{M}_{\rm Edd}$, as is the case here (Fisker et al. 2004).

Considering the relatively limited PRE of the present burst, it seems that only a part of the neutron star surface is involved during the first peak of the burst. Strong convective mixing does likely occur during this peak, which eventually leads, after

touch-down, to the ignition of the unburned material, and thus a second brightening. In a more exotic interpretation one might presume that the double peaks are the result of two bursts occurring nearly simultaneously on the stellar surface. However, we can rule out this model because matter needs to be confined to a small region, which is only possible in the case of magnetized neutron stars, with field strengths $\geqslant 10^9$ G (Cavecchi et al. 2011 and reference therein). For the given magnetic field $(0.5–1.6) \times 10^8$ G of 4U 1608–52 (Asai et al. 2013), the flame should easily spread out and produce a single-peak burst profile.

In summary, we have discussed plausible scenarios to explain the double-peaked burst from the source 4U 1608–52. The low-energy capability of *NICER* enables us for the first time to rule out absorption effects as the origin of the dip, as proposed earlier. The possibility of shear instability, thermonuclear flame spreading, or nuclear waiting points applicable to non-PRE bursts can fit the picture. We also favor the scenario of additional burning in the cooling tail of the burst, considering the temperature evolution across the burst. The reburning would be feasible only if residual or fresh material lies above the cold fuel as a result of hydrodynamical instabilities.

It is interesting to note that the scaling factor (f_a) goes down at the time of the dip. It thus appears that reprocessing of the burst emission by the accretion disk halts temporarily at this phase. If the inner disk is somehow briefly affected during the PRE process (perhaps due to Poynting–Robertson drag), a reduction of the reflected burst flux would also lower the observed flux (Fragile et al. 2018). Nonetheless, we can rule out this possibility as the dip occurs a few seconds after the PRE phase. A substantial fraction of the observed burst flux is also expected to be scattered off the inner disk that could produce the secondary peak (see, Lapidus & Sunyaev 1985; He & Keek 2016 and references therein). However, this idea may be discarded because the accretion proceeds forward during the burst as shown by the increasing f_a.

ORCID iDs

Gaurava K. Jaisawal https://orcid.org/0000-0002-6789-2723
Jérôme Chenevez https://orcid.org/0000-0002-4397-8370
Jean J. M. in't Zand https://orcid.org/0000-0002-4363-1756
Duncan K. Galloway https://orcid.org/0000-0002-6558-5121
Tod E. Strohmayer https://orcid.org/0000-0001-7681-5845
Tolga Güver https://orcid.org/0000-0002-3531-9842
Diego Altamirano https://orcid.org/0000-0002-3422-0074
Deepto Chakrabarty https://orcid.org/0000-0001-8804-8946
Sebastien Guillot https://orcid.org/0000-0002-6449-106X
Renee M. Ludlam https://orcid.org/0000-0002-8961-939X
Christian Malacaria https://orcid.org/0000-0002-0380-0041

References

Arnaud, K. A. 1996, in ASP Conf. Ser. 101, Astronomical Data Analysis Software and Systems, ed. G. H. Jacoby & J. Barnes (San Francisco, CA: ASP), 17
Asai, K., Matsuoka, M., Mihara, T., et al. 2013, ApJ, 773, 117
Bagnoli, T., in't Zand, J. J. M., Patruno, A., & Watts, A. L. 2014, MNRAS, 437, 2790
Ballantyne, D. R. 2004, MNRAS, 351, 57
Belian, R. D., Conner, J. P., & Evans, W. D. 1976, ApJL, 206, L135
Bhattacharyya, S., & Strohmayer, T. E. 2006, ApJL, 636, L121
Bult, P., Altamirano, D., Arzoumanian, Z., et al. 2018, ApJL, 860, L9
Cavecchi, Y., Patruno, A., Haskell, B., et al. 2011, ApJL, 740, L8
Chen, Y.-P., Zhang, S., Zhang, S.-N., Li, J., & Wang, J.-M. 2012, ApJL, 752, L34
Degenaar, N., Ballantyne, D. R., Belloni, T., et al. 2018, SSRv, 214, 15
Done, C., Gierliński, M., & Kubota, A. 2007, A&ARv, 15, 1
Ebisuzaki, T., Hanawa, T., & Sugimoto, D. 1983, PASJ, 35, 17
Fisker, J. L., Thielemann, F.-K., & Wiescher, M. 2004, ApJL, 608, L61
Fragile, P. C., Ballantyne, D. R., Maccarone, T. J., & Witry, J. W. L. 2018, ApJL, 867, L28
Fujimoto, M. Y., & Gottwald, M. 1989, MNRAS, 236, 545
Fujimoto, M. Y., Sztajno, M., Lewin, W. H. G., & van Paradijs, J. 1988, A&A, 199, L9
Galloway, D. K., & Keek, L. 2017, arXiv:1712.06227
Galloway, D. K., Muno, M. P., Hartman, J. M., Psaltis, D., & Chakrabarty, D. 2008, ApJS, 179, 360
Gendreau, K., & Arzoumanian, Z. 2017, NatAs, 1, 895
Gendreau, K. C., et al. 2016, Proc. SPIE, 9905, 99051H
Grindlay, J., & Gursky, H. 1976, ApJL, 209, L61
Grindlay, J. E., & Liller, W. 1978, ApJL, 220, L127
Güver, T., Özel, F., Cabrera-Lavers, A., & Wroblewski, P. 2010, ApJ, 712, 964
He, C.-C., & Keek, L. 2016, ApJ, 819, 47
Inogamov, N. A., & Sunyaev, R. A. 1999, AstL, 25, 269
in't Zand, J. J. M., Galloway, D. K., Marshall, H. L., et al. 2013, A&A, 553, A83
Jahoda, K., Markwardt, C. B., Radeva, Y., et al. 2006, ApJS, 163, 401
Ji, L., Zhang, S., Chen, Y., et al. 2014a, ApJL, 791, L39
Ji, L., Zhang, S., Chen, Y.-P., et al. 2014b, A&A, 564, A20
Kajava, J. J. E., Koljonen, K. I. I., Nättilä, J., Suleimanov, V., & Poutanen, J. 2017, MNRAS, 472, 78
Keek, L., Arzoumanian, Z., Bult, P., et al. 2018a, ApJL, 855, L4
Keek, L., Arzoumanian, Z., Chakrabarty, D., et al. 2018b, ApJL, 856, L37
Keek, L., & Heger, A. 2017, ApJ, 842, 113
Keek, L., in't Zand, J. J. M., Kuulkers, E., et al. 2008, A&A, 479, 177
Kuulkers, E., den Hartog, P. R., in't Zand, J. J. M., et al. 2003, A&A, 399, 663
Kuulkers, E., Homan, J., van der Klis, M., Lewin, W. H. G., & Méndez, M. 2002, A&A, 382, 947
Lapidus, I. I., & Sunyaev, R. A. 1985, MNRAS, 217, 291
Lewin, W. H. G., Vacca, W. D., & Basinska, E. M. 1984, ApJL, 277, L57
Lewin, W. H. G., van Paradijs, J., & Taam, R. E. 1993, SSRv, 62, 223
Mitsuda, K., Inoue, H., Koyama, K., et al. 1984, PASJ, 36, 741
Muno, M. P., Chakrabarty, D., Galloway, D. K., & Savov, P. 2001, ApJL, 553, L157
Özel, F., Psaltis, D., Güver, T., et al. 2016, ApJ, 820, 28
Penninx, W., Damen, E., Tan, J., Lewin, W. H. G., & van Paradijs, J. 1989, A&A, 208, 146
Poutanen, J., Nättilä, J., Kajava, J. J. E., et al. 2014, MNRAS, 442, 3777
Prigozhin, G., Gendreau, K., Foster, R., et al. 2012, Proc. SPIE, 8453, 845318
Spitkovsky, A., Levin, Y., & Ushomirsky, G. 2002, ApJ, 566, 1018
Strohmayer, T., & Bildsten, L. 2003, arXiv:astro-ph/0301544
Suleimanov, V., Poutanen, J., & Werner, K. 2012, A&A, 545, A120
Tananbaum, H., Chaisson, L. J., Forman, W., Jones, C., & Matilsky, T. A. 1976, ApJL, 209, L125
van Straaten, S., van der Klis, M., & Méndez, M. 2003, ApJ, 596, 1155

Wachter, S., Hoard, D. W., Bailyn, C. D., Corbel, S., & Kaaret, P. 2002, ApJ, 568, 901

Walker, M. A. 1992, ApJ, 385, 642

Wilms, J., Allen, A., & McCray, R. 2000, ApJ, 542, 914

Worpel, H., Galloway, D. K., & Price, D. J. 2013, ApJ, 772, 94

Worpel, H., Galloway, D. K., & Price, D. J. 2015, ApJ, 801, 60

Zhang, G., Méndez, M., Altamirano, D., Belloni, T. M., & Homan, J. 2009, MNRAS, 398, 368